Spatial Decomposition of Climate Feedbacks in the Community Earth System Model

A. GETTELMAN, J. E. KAY, AND J. T. FASULLO

National Center for Atmospheric Research, Boulder, Colorado*

(Manuscript received 26 July 2012, in final form 24 October 2012)

ABSTRACT

An ensemble of simulations from different versions of the Community Atmosphere Model in the Community Earth System Model (CESM) is used to investigate the processes responsible for the intermodel spread in climate sensitivity. In the CESM simulations, the climate sensitivity spread is primarily explained by shortwave cloud feedbacks on the equatorward flank of the midlatitude storm tracks. Shortwave cloud feedbacks have been found to explain climate sensitivity spread in previous studies, but the location of feedback differences was in the subtropics rather than in the storm tracks as identified in CESM. The cloud-feedback relationships are slightly stronger in the winter hemisphere. The spread in climate sensitivity in this study is related both to the cloud-base state and to the cloud feedbacks. Simulated climate sensitivity is correlated with cloud-fraction changes on the equatorward side of the storm tracks, cloud condensate in the storm tracks, and cloud microphysical state on the poleward side of the storm tracks. Changes in the extent and water content of stratiform clouds (that make up cloud feedback) are regulated by the base-state vertical velocity, humidity, and deep convective mass fluxes. Within the storm tracks, the cloud-base state affects the cloud response to CO_2-induced temperature changes and alters the cloud feedbacks, contributing to climate sensitivity spread within the CESM ensemble.

1. Introduction

Global climate change is often described with a simple metric of the temperature response to a given radiative forcing of the climate system, the climate sensitivity γ. The range of climate sensitivity to a doubling of carbon dioxide (CO_2) simulated by general circulation models (GCMs) of 2.1–4.4 K has changed only slightly in 30 years (Charney 1979; Solomon et al. 2007), with a most likely value of ~3 K (Meehl et al. 2007b), recently updated to 3.3 K (Huber et al. 2011). Observations and models have been used to help understand climate feedbacks that determine the climate sensitivity, such as water vapor (Soden et al. 2002; Gettelman and Fu 2008), clouds (Dessler 2010), and albedo feedback (Flanner et al. 2011).

Recent work has attempted to link climate sensitivity to model parameters in large parameter perturbation experiments (Piani et al. 2005; Sanderson et al. 2010), multimodel ensembles (Rougier et al. 2009), or targeted perturbations to a single model (Yoshimori et al. 2011; Gettelman et al. 2012; Watanabe et al. 2012). Webb et al. (2012) provide an extensive summary of recent experiments. The spread in simulated climate sensitivity results largely from differences in cloud feedbacks (Bony et al. 2006; Soden and Held 2006; Dufresne and Bony 2008), particularly the shortwave (SW) feedbacks due to low clouds (Williams and Webb 2009; Soden and Vecchi 2011; Webb et al. 2012) in the subtropics. Zelinka et al. (2012a) noted that there is also considerable spread in high cloud feedbacks, but they contribute less to uncertainty in net cloud feedback because of compensating SW and longwave (LW) effects. Tsushima et al. (2006) linked changes in climate sensitivity to changes in cloud water and cloud ice content.

Several studies have also looked at the spatial distribution of climate feedbacks. Colman (2002) examined feedbacks spatially (but with fixed cloud optical properties). Ogura et al. (2008) found sensitivity in a single GCM was altered by changes to ice microphysics in the

* The National Center for Atmospheric Research is sponsored by the National Science Foundation.

Corresponding author address: A. Gettelman, National Center for Atmospheric Research, 1850 Table Mesa Dr., Boulder, CO 80305.
E-mail: andrew@ucar.edu

DOI: 10.1175/JCLI-D-12-00497.1

© 2013 American Meteorological Society

Southern Hemisphere storm track. Soden and Vecchi (2011) looked at the spatial distribution of feedbacks in a multimodel ensemble, and Taylor et al. (2011a) decomposed feedbacks spatially in a single GCM. Taylor et al. (2011b) examined the seasonality of feedbacks.

This study uses experiments from an atmosphere–ocean GCM to explore which feedbacks determine climate sensitivity and what processes affect these feedbacks through different generations of a single GCM "family." This has the advantage of tight constraints on the system and detailed diagnostics. The use of a single model with perturbation experiments has the disadvantage of limited structural uncertainty. We confirm that cloud feedbacks are critical to the spread of climate sensitivity. We seek to understand what regions and regimes are most important for this spread, and whether we can relate cloud feedbacks and climate sensitivity to model state and physical (cloud) processes. Method (section 2) and models (section 3) are defined below. Results are in section 4. The paper finishes with a discussion of physical mechanisms (section 5) and conclusions (section 6).

2. Method

We will diagnose climate feedbacks and climate sensitivity in a suite of GCM experiments, and then explore how the variability is correlated with model states.

a. Sensitivity and feedbacks

We use the radiative kernel method (Soden and Held 2006) to estimate climate feedbacks. The method has been shown to reproduce feedbacks calculated with detailed partial radiative perturbation (PRP) calculations (Soden et al. 2008). The notation and method here follow Gettelman et al. (2012).

Climate sensitivity γ (K) is the change in global average surface temperature that results from an imposed radiative forcing G (W m^{-2}):

$$\gamma = G/\lambda\,, \tag{1}$$

where λ is the feedback parameter (W m^{-2} K^{-1}). If one assumes a linear and independent interaction of feedbacks, λ is the sum of a series of X feedbacks ($\lambda = \sum \lambda_X$) (Colman 2003; Soden et al. 2008). Each λ_X can be decomposed into a *radiative kernel* (Soden et al. 2008) $\partial R/\partial X$, where ∂R is the change in top-of-atmosphere (TOA) energy balance R for a unit perturbation ∂X, and a *climate response* $\Delta X/\Delta T_{\rm as}$, where ΔX and $\Delta T_{\rm as}$ are the difference in X and the near-surface temperature $T_{\rm as}$ from a pair of simulations, one with imposed forcing G. Radiative kernels are derived from Shell et al. (2008). Sanderson and Shell (2012) have noted the dependence of the kernel on model state, especially the surface albedo kernel, and this effect is discussed further below.

The kernel method does not allow a direct estimate of cloud feedbacks. Cloud feedbacks are calculated by adjusting the cloud radiative effect (CRE) change (ΔCRE) for changes in model state that affect TOA fluxes. Since CRE = $R_{\rm cld} - R_{\rm clr}$ (where subscripts cld and clr indicate cloudy and clear skies, respectively), changes to $R_{\rm clr}$, from, for example, surface albedo or water vapor changes, would affect CRE and cloud feedback ($\lambda_{\rm cld} = \Delta{\rm CRE}/\Delta T_{\rm as}$). Kernel adjusted cloud feedback (Soden et al. 2008; Shell et al. 2008), or ACF, uses radiative kernels to correct ΔCRE for changes to the model state (other feedbacks). Taylor et al. (2011a), using the Community Climate System Model, version 3 (CCSM3), noted that the ACF yields global and regional results that are similar to the PRP estimate of cloud feedbacks. The correction is weakly dependent on the Community Atmosphere Model, version 3 (CAM3), cloud distribution and is only significant at high latitudes, where CAM3 and CAM5 have different cloud masking of the surface albedo kernel (Sanderson and Shell 2012), but this fact does not alter the conclusions of this paper because the area involved is small. Zelinka et al. (2012a) have developed cloud-property kernels to explore changes due to cloud amount and optical depth. Necessary outputs were not available from these simulations to use the cloud-property kernels, but ACF results derived from these experiments by Gettelman et al. (2012) compare well with those derived with the cloud-property kernels of Zelinka et al. (2012b), and our analysis does enable an understanding of cloud-fraction changes.

To estimate the climate sensitivity γ from runs that are out of balance ($\Delta R \neq 0$, which occurs with fixed sea surface temperatures), we calculate an effective sensitivity parameter $\gamma_{\rm eff}$ (Gettelman et al. 2012). By using the total change in forcing between two runs with different surface temperatures and CO_2,

$$\gamma_{\rm eff} = \frac{G_{\rm CO2}}{(G_{\rm CO2} + \Delta R)} \Delta T_{\rm as}\,, \tag{2}$$

where $G_{\rm CO2}$ is the radiative forcing for doubling CO_2 from 280 to 560 ppm by volume (ppmv). The radiative forcing $G_{\rm CO2}$ is approximately 3.7 W m^{-2} (Solomon et al. 2007) but varies in each model by 10% ($\approx$0.2 W m^{-2}) because of differences in state and radiation code (Kay et al. 2012b). We find $G_{\rm CO2} = 3.9$ W m^{-2} from estimating the forcing from a fixed SST experiment with only CO_2 doubled from 367 to 734 ppmv for CAM5 [following the method of Hansen et al. (2002)]. In Eq. (2), ΔR (positive downward) is the TOA imbalance. For equilibrium

simulations, $\Delta R = 0$ and $\gamma_{\text{eff}} = \Delta T_{\text{as}}$. Gettelman et al. (2012) have shown that $\gamma_{\text{eff}} \approx \gamma$.

Note that our analysis includes both the ''fast response'' of the system to CO_2 increases before the surface temperature has time to adjust and the slow response to the change in SST (Hansen et al. 2002). The latter (slow response) is usually taken to be ''feedback,'' and the former is included in the ''forcing'' (Gregory and Webb 2008). We have performed separate calculations with SST changes only (feedback or slow response) to verify that, for cloud feedbacks, almost all of the response is due to the SST change alone. The net (LW + SW) ΔCRE changes by 1.14 W m^{-2} for doubling CO_2 and changing SST together and by 1.21 W m^{-2} for changing SST only (feedback), whereas the CO_2-only (fast response) change is -0.02 W m^{-2}. Thus, the fast response is small. Since we are mostly concerned with the differences between simulations with the same CO_2 perturbation, using the total response should not affect the feedback analysis.

b. Correlation/regression analysis

The analysis will first relate climate sensitivity to feedbacks. We use linear correlation analysis to relate global mean feedback values to climate sensitivity. Similar analysis methods are used by Soden and Vecchi (2011) and Zelinka et al. (2012a). The results are spatially coherent, leading naturally to a discussion of particular physical regimes. The current analysis confirms that cloud feedbacks are a critical source of intermodel spread in climate sensitivity, and therefore we focus on parameters that are related to cloud radiative effects and explore how specific properties of clouds in the simulations are related to the climate sensitivity. Cloud radiative properties are evaluated, and then three areas are highlighted: 1) moisture in and around clouds (humidity and cloud water path), 2) the dynamic environment around stratiform and convective clouds (large-scale vertical velocity, stability, and convective mass fluxes), and 3) cloud microphysical properties (particle size and number).

Two outputs from a linear regression are used, the correlation, or variance explained, and the regression slope s, or magnitude explained. If climate sensitivity is related to parameter X by $\gamma \propto sX$, then X is only important if s is significantly different from zero. Statistical significance is defined by the 95% confidence interval of a two-sided t test. Even if linear regressions are not perfect analysis tools, they provide guidance as to parameters and regions that are important for explaining variance (or spread). We highlight significant global and regional correlations and large slopes as potential indicators of processes that are important for explaining global climate sensitivity. Note that the units of the regression slopes are different for different parameters. Also note that correlation does not imply causation and could just be that both sensitivity and a parameter are correlated with another parameter. In contrast, global and regional relationships with insignificant correlations and slopes are unlikely to be related to climate sensitivity.

We produce maps that are based on both mean values from the simulations and differences between preindustrial and future (doubled atmospheric CO_2 concentration) simulations. As a regressor X, we use 1) feedbacks, 2) mean base state from the $1 \times CO_2$ simulations of selected variables, and 3) differences between $2 \times CO_2$ and $1 \times CO_2$ simulations of selected variables. These latter differences will be estimated as the percent difference per degree of change in local surface temperature T_s (% K^{-1}) to try to isolate critical processes that might respond to temperature. Results are not strongly dependent on the exact normalization procedure of the differences.

3. Models and experiments

a. CESM description

The model used in this study is the Community Earth System Model (CESM) of the National Center for Atmospheric Research (NCAR). We focus on changes between two versions of the CAM in CESM: version 4 (CAM4) and version 5 (CAM5). CAM4 is essentially the same as NCAR CAM3 (Collins et al. 2004, 2006) with modifications to the deep convective closure and momentum transport (Neale et al. 2008). CAM5 includes a substantially revised physical parameterization suite relative to CAM4 (Gettelman et al. 2010; Neale et al. 2010). The only major moist physics parameterization remaining constant between CAM4 and CAM5 is the deep convective parameterization (Neale et al. 2008), and thus, they represent very different models.

b. Experiment description

To explore these sensitivities across a range of parameterizations, we use a suite of experiments with different versions of CESM. The experiments contain pairs of simulations for preindustrial (284.7 ppm) and doubled (569.4 ppm) values of CO_2. Experiments are run with a Slab Ocean Model (SOM) or with fixed SST and a specified $2 \times CO_2$ SST perturbation from the climatological mean, following the method of Gettelman et al. (2012) and similar to Cess et al. (1989). There are a total of 8 SOM and 13 fixed-SST experiment simulation pairs, which are listed in Table 1 along with their γ_{eff}. Details of the experiments are described in the

TABLE 1. Description of runs used in this study and their effective climate sensitivity γ_{eff}. Run types are either SOM or modified Cess, with horizontal resolution of either 0.9° × 1.25° (shown as 1°) or 1.9° × 2.5° (shown as 2°) as described in the text.

Name	Type	Resolution	Description	γ_{eff}
CAM4-SOM	SOM	1°	CAM4 physics	3.1
CAM4-SOM2	SOM	2°	CAM4 physics	3.1
CAM5-SOM	SOM	1°	CAM5 physics	4.0
CAM5-SOM2	SOM	2°	CAM5 physics	4.2
CAM5-SOMa	SOM	1°	CAM5 physics, 1850 aerosols	4.5
CAM5-SOM2 1	SOM	2°	CAM5.0α1 physics	4.4
CAM5-SOM2 2	SOM	2°	CAM5.0α2 physics	5.7
CAM5-SOM2 3	SOM	2°	CAM5.0α3 physics	4.2
CAM4-Cess	Cess	2°	CAM4 physics = CAM4–SOM2	2.8
+micro	Cess	2°	CAM4 physics + new microphysics (RH_c = 0.92)	2.7
+micro2	Cess	2°	CAM4 physics + new microphysics (RH_c = 0.88)	2.4
+macro	Cess	2°	Above + new macrophysics	2.9
+rad	Cess	2°	Above + new radiation and cloud optics	3.7
+aero	Cess	2°	Above + new aerosol scheme	3.5
+PBL	Cess	2°	Above + new PBL (RH_c = 0.95)	2.9
+PBL2	Cess	2°	Above + new PBL (RH_c = 0.91)	2.7
CAM5-Cessα1	Cess	2°	Above + new ShCu scheme = CAM5–SOM2α1	4.4
CAM5-Cessα2	Cess	2°	CAM5–SOM2α2	5.5
CAM5-Cess ΔSST4	Cess	2°	CAM5–Cess with different ΔSST	4.8
CAM5-Cess Aero	Cess	2°	Fixed aerosol mass and number	4.5
CAM5-Cess Conv	Cess	2°	Modified deep convective LWP for radiation	5.4

appendix. The major set of experiments progressively changes parameterizations between CAM4 and CAM5.

In total there are 21 simulation pairs representing a diversity of parameterizations (structural uncertainty) and model adjustment experiments (parameter uncertainty) from two versions of an atmospheric GCM (CAM version 4 and 5) with different physical parameterization suites in the same earth system model (CESM). We note the caveat that we are not analyzing coupled simulations in this ensemble, using only Slab Ocean Model and uncoupled experiments to focus on fast feedbacks. This small ensemble falls between previous work looking at large ensembles from a single model (Piani et al. 2005; Sanderson et al. 2008; Rougier et al. 2009) or multimodel analyses (Knutti et al. 2006; Soden and Vecchi 2011; Webb et al. 2012).

Figure 1 shows the zonal annual mean climatological values of longwave (Fig. 1a) and shortwave (Fig. 1a) CRE from all 21 base (1 × CO_2) runs in comparison with satellite observations from the Energy Balance Adjusted Flux (EBAF) product, version 2.6, from the Clouds and the Earth's Radiant Energy System satellite instrument (Loeb et al. 2009). There are significant differences between the simulations (up to 40 W m^{-2} in the SW component in the tropics, partially balanced by the LW), and some systematic biases. All of the simulations

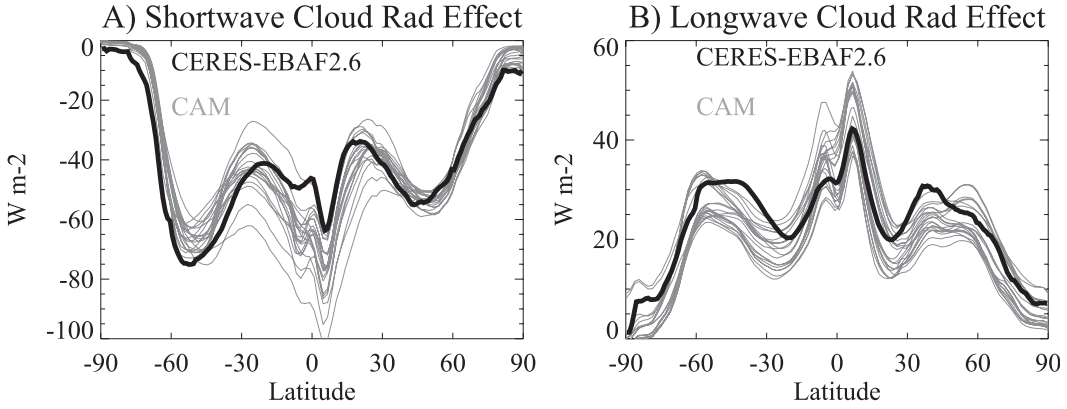

FIG. 1. Zonal annual mean climatological values of (a) SW and (b) LW cloud radiative forcing from all 21 base (1 × CO_2) runs (gray lines) and satellite observations (thick black line) from the EBAF product (Loeb et al. 2009).

TABLE 2. Table of correlations between γ_{eff} and listed feedbacks for CAM simulation pairs. Correlations that are statistically significant on the basis of a two-sided t test at the 95% level are marked with an asterisk. Also shown are the fraction of variance r^2 explained by the linear correlation and the regression slope (W m^{-2} K^{-2}). Feedbacks are described in the text.

Feedback	Mean Correlation	r^2	Slope
Net cloud	0.67*	0.44	0.07
LW cloud	−0.90*	0.80	−0.09
SW cloud	0.84*	0.71	0.16
Albedo	−0.56*	0.32	−0.01
H2O + LR	0.21	0.04	−0.006
TEMP	−0.11	0.01	−0.01
TS	−0.45	0.20	−0.006

represent ''Earthlike'' states, however, with storm tracks and significant equatorial cloudiness, with good qualitative agreement with the observations. Other metrics of the simulations that we discuss broadly resemble other model estimates: for example, the cloud feedbacks in the simulations (see Gettelman et al. 2012, their Fig. 6) resemble kernel ACFs from models in the Coupled Model Intercomparison Project, phase 3 (CMIP3; Meehl et al. 2007a), calculated by Soden and Vecchi (2011) or similar experiments in the Cloud Feedback Model Intercomparison Project, phase 1 (CFMIP1; Zelinka et al. 2012b).

4. Results

First, we analyze feedbacks in the 21 CESM experiments. We will then look at the relationship between sensitivity and feedbacks or model state in the CESM simulations, focusing on cloud radiative properties, cloud water and ice, the dynamics around clouds, and then cloud microphysics.

a. CESM feedbacks

First, we consider feedbacks listed in Table 2 by following previous work (Colman 2003; Soden et al. 2008). Figure 2 illustrates a statistically significant correlation for the CAM simulations between γ_{eff} and the kernel ACFs divided into SW-feedback (ASCF; Fig. 2a) and LW-feedback (ALCF; Fig. 2b) components. Each point represents one of 21 experiment pairs. The LW correlation is −0.90 (slope −0.09 W m^{-2} K^{-2}), which explains 80% of the variance (Table 2). For the SW, the correlation is 0.84 ($r^2 = 0.71$) and the slope is 0.16 W m^{-2} K^{-2}. When compared with ASCF, ALCF has a similar correlation but a smaller slope; that is, the variation in LW feedback produces smaller changes in sensitivity than do changes in the SW feedback. The physical interpretation is that ALCF has a tighter fit but is less important for explaining the magnitude (or spread) of the climate sensitivity than is ASCF. This is consistent with theories that LW cloud feedback is positive because of constant tropical cloud-top emission temperature (Zelinka and Hartmann 2010). Globally, ASCF and ALCF are anticorrelated with each other (Fig. 2). This anticorrelation arises from specific regimes and locations, discussed below and shown in Fig. 3. This relationship is seen in CMIP3 models (Soden and Vecchi 2011). The anticorrelation and fact that ASCF has a larger slope when regressed against climate sensitivity than does ALCF

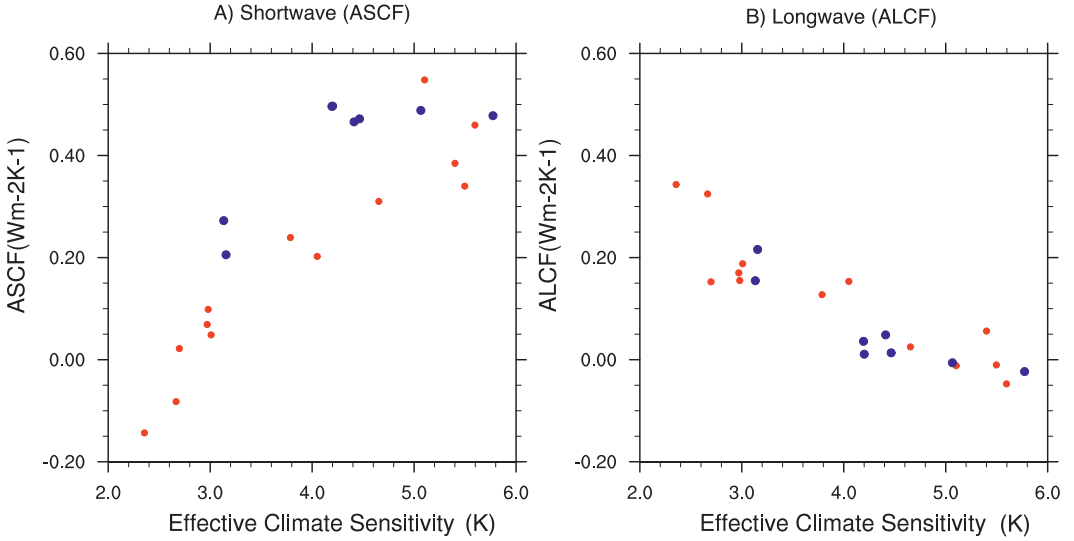

FIG. 2. Effective climate sensitivity γ_{eff} vs (a) ASCF and (b) ALCF from CAM experiment pairs. SOM experiments are in blue, and modified Cess experiments are in red.

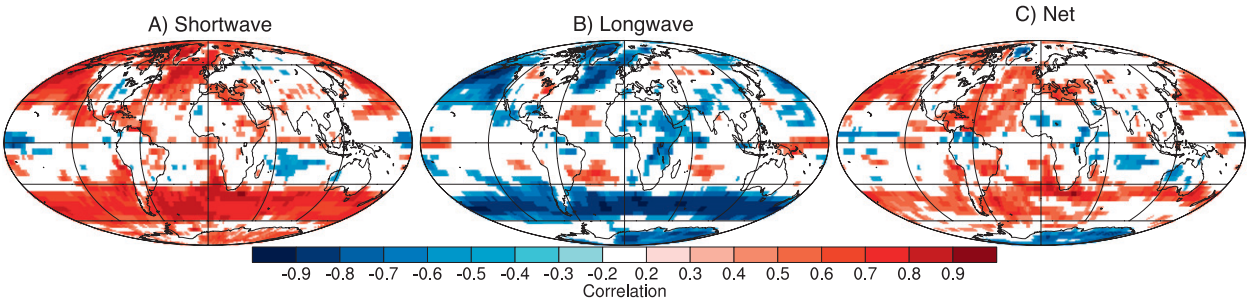

FIG. 3. Pattern correlations of γ_{eff} with cloud feedbacks at each point from 21 CAM experiments for (a) SW, (b) LW, and (c) net cloud feedback.

indicates that clouds with both LW and SW (but stronger SW) effects (Webb et al. 2006) are important for explaining climate-sensitivity magnitude. The magnitude of the ASCF slope is nearly 2 times that of ALCF, so that the net cloud feedback (ACF) correlation is positive (Table 2).

The evolution of γ_{eff} in the simulations between CAM4 and CAM5 is described by Gettelman et al. (2012) and can be deduced from Fig. 2 and Table 1. Two groups of SOM experiments represent CAM4 (low γ_{eff}) and CAM5 (high γ_{eff}). Sensitivities larger than 3.5 K correspond to runs in which the new radiation code is used, and sensitivities larger than 4 K are all simulations with the CAM5 shallow convection scheme.

Correlations and slopes from this ensemble for the major climate feedbacks λ_X are listed in Table 2. Albedo feedbacks are significantly correlated with sensitivity, but the small slope confirms that albedo feedbacks do not explain the spread in sensitivity. Lapse-rate (LR) feedbacks are estimated by subtracting a constant temperature change with height from the total temperature feedback (TEMP) by following the method of Soden et al. (2008). Water vapor (H_2O) and LR feedbacks are less variable across models when combined than separately (Colman 2003; Soden et al. 2008), and these are not well correlated with γ_{eff}. The surface temperature feedback (TS) is large (Soden et al. 2008) but not well correlated with γ_{eff}. These results are consistent with previous analyses of multimodel ensembles (Williams and Webb 2009) and single model parameterization sweep experiments (Rougier et al. 2009), showing that cloud feedbacks dominate the climate sensitivity spread in models.

We decompose the global regression spatially to explore which locations dominate the spread (regression slope) in cloud feedbacks. Following the regional decomposition of Webb et al. (2012), we set the cloud feedbacks equal to the ensemble mean cloud feedback outside a target region. The method isolates the correlation contribution to specific regions, as the correlation outside the region is zero, and the results are broadly linear: the regional slopes in each region sum to the global regression slope. Regions are the tropics within 30° of the equator, the midlatitudes (30°–55°N/S) and high latitudes poleward of 55°N/S. Area weights are applied. The tropics contribute only 20% to the regression, despite being 50% of the area, while the midlatitudes (with 30% of the area) contribute ~60% and the high latitudes (20% area) contribute also 20% to the regression for LW (ALCF), SW (ASCF), and net (ACF) feedbacks. This is a similar breakdown to the regional analysis for SW and net feedbacks in Gettelman et al. (2012, their Fig. 7) for the mean feedback contribution. The regression has higher weight in the midlatitudes, indicating that the spread of sensitivity resulting from the change in feedback is more dependent on the midlatitudes. The prominence of midlatitudes is different than in other models (Webb et al. 2012) and multimodel analyses (Soden and Vecchi 2011). However, using a similar decomposition, (Webb et al. 2012) also found that CCSM3, the predecessor model to CESM, has a large contribution to sensitivity from midlatitudes. We investigate these differences further below.

By repeating the correlation between the feedbacks at each point and the global average climate sensitivity, the regimes (locations) critical for relating feedbacks to climate sensitivity in CESM can be identified. Albedo feedbacks have locally strong correlations with climate sensitivity (not shown) around the sea ice (and Northern Hemisphere seasonal snow) edge, but none of the other noncloud feedbacks in Table 2 have strong regional correlations.

Figure 3 illustrates local correlations for cloud feedbacks with global climate sensitivity γ_{eff}. Figure 3 and subsequent map figures are derived by interpolating each experiment to a standard grid, then performing a regression at each point against global γ_{eff} (linear regression on data similar to Fig. 2 at each point) and mapping the correlation (Fig. 3) or regression slope (Fig. 5, described below). The value plotted in Fig. 3 is the

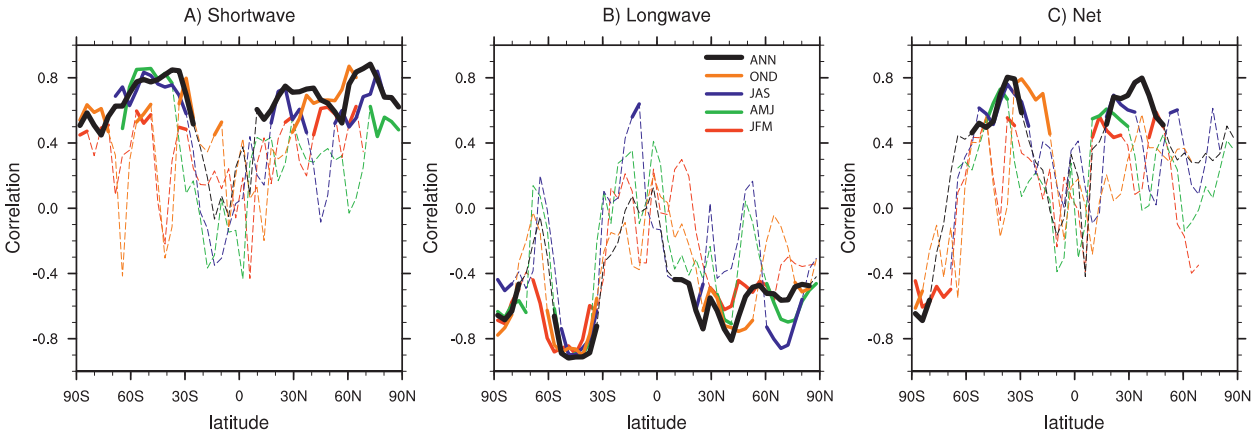

FIG. 4. Zonal mean seasonal correlations of γ_{eff} with cloud feedbacks at each point from 21 CAM experiments for (a) SW, (b) LW, and (c) net cloud feedback. Thick lines are statistically significant. Annual mean is shown in black. ANN indicates annual, and three-month periods are labeled by the first letter of each month therein.

correlation across simulations of the local cloud feedback with the global γ_{eff} for the 21 experiment pairs. For this and all subsequent map figures, white colors indicate regions where correlations are not statistically different from zero.

Figure 3 illustrates that the global correlations in Fig. 2 arise mostly in the storm tracks in both hemispheres. Correlations are also clear in the annual zonal mean (Fig. 4, black line). There is strong regional cancellation between the SW (Figs. 3a, 4a) and the LW (Figs. 3b, 4b). The anticorrelation occurs in the same regions (especially the storm tracks), indicating reductions in clouds with SW and LW effects on the equatorward branches of the storm tracks. Stratocumulus transition regions off the eastern coasts of South America, Africa, and North America also show up without LW effects, indicating low stratus clouds. However, their area is small. The transition regions do not show up in the zonal mean net feedback (Fig. 4c), and they do not exert strong leverage on the global correlations (Gettelman et al. 2012). The SW feedbacks extend farther into the subtropics, down to 30° latitude. The result is that the strongest correlation between net cloud feedbacks (Fig. 3c) and climate sensitivity is found on the equatorward flank of the storm track at 30°–60°N/S (Fig. 4c).

In Fig. 4, cloud feedbacks are also decomposed by season. There are small seasonal differences in correlations (or regression slopes, not shown) between cloud feedbacks and climate sensitivity. Correlations between SW cloud feedbacks and climate sensitivity (Fig. 4a) are slightly higher in the winter hemisphere. There are hints of a different seasonality in the tropics. Taylor et al. (2011b) note that SW cloud feedback in CCSM3 is larger in boreal summer in the tropics, similar to Fig. 4a. In the LW (Fig. 4b) there is virtually no annual cycle, but the Northern Hemisphere has stronger LW feedbacks in summer. These effects are the opposite seasonal sign of the mean CRE, where the SW peaks in summer and the LW peaks in winter. Smaller seasonal-CRE-magnitude seasons seem to be more correlated with sensitivity.

Following Soden and Vecchi (2011) we also examine the regression of the local cloud feedback at each point with the global cloud feedback, as a different measure of the regions contributing to the spread in cloud feedbacks (Fig. 5). The regression slope between the local feedback and the climate sensitivity (W m^{-2} K^{-1}) looks similar to the correlations in Fig. 3, with the storm-track regions and the subtropical oceans contributing prominently to spread. However, the figure is significantly different than a similar analysis from Soden and Vecchi (2011, their Fig. 4), using CMIP3 models, which shows the largest spread in cloud feedback in the subtropics and the transition regions from stratocumulus to trade cumulus. The CESM ensemble does highlight the subtropical oceans and the Northern Hemisphere storm tracks, similar to Soden and Vecchi (2011). The CESM ensemble does not highlight the transition regions from stratocumulus to cumulus clouds in the subtropics (at 20°N and 20°S), despite a different sign of cloud feedbacks in these subtropical transition regions between CAM4 and CAM5 (Gettelman et al. 2012, their Fig. 6). It is also interesting that there is no relationship between local and global feedbacks in the CMIP3 models in the Southern Ocean in Soden and Vecchi (2011), where CESM shows significant regression slope and where other analyses of CMIP3 models show significant correlations of clouds with climate sensitivity (Trenberth and Fasullo 2010) and clouds, subsidence, and humidity (Fasullo and Trenberth 2012).

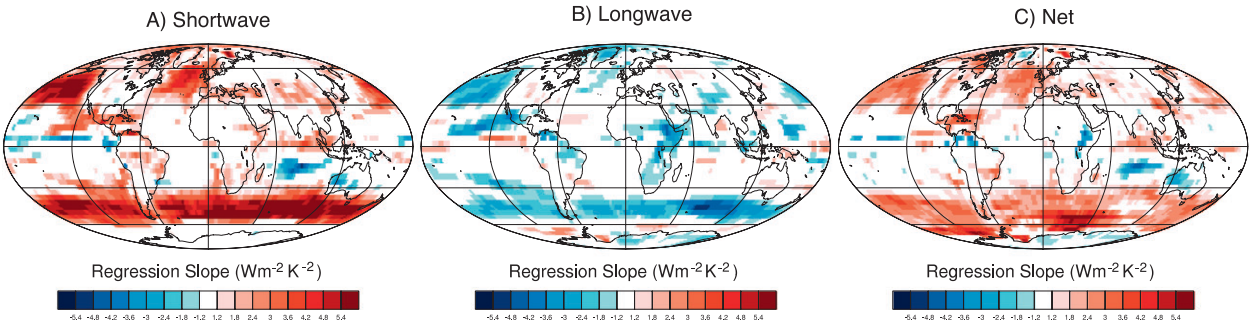

FIG. 5. Regression coefficient of γ_{eff} with cloud feedbacks (W m^{-2} K^{-1}) at each point from 21 CAM experiments for (a) SW, (b) LW, and (c) net cloud feedback.

b. CESM model state

To better understand the physical mechanisms that give rise to these feedback correlations in the CESM simulations, we can look at critical aspects of the model state that define clouds. We group these parameters into categories that we discuss in more detail: radiative properties (cloud radiative effect and cloud occurrence), moisture properties (liquid and ice water path; relative humidity), dynamics of clouds (vertical velocity, stability, and convective mass flux), and cloud microphysical properties (number concentration and particle size). Table 3 shows global regressions across the 21 experiments between γ_{eff} and properties of 1) the mean base ($1 \times CO_2$) state of each parameter, 2) the percent change between present and doubled-CO_2 conditions for each parameter, and 3) the percent change per degree of local warming. The last two (methods 1 and 2) are essentially the same when the local and global temperature changes are related. Normalizing by local changes in temperature (method 3) allows isolation of process changes relative to local (rather than global) changes in the experiment pairs. It also facilitates comparisons between models with prescribed local surface temperature perturbations. The correlations and slopes are generally similar between methods 2 and 3, both globally (Table 3) and locally. We also perform regression analysis at every point separately so that the critical regions or regimes for each parameter can be explored. Global regressions are not performed for vertical velocity, since the global integral is zero.

c. Radiative properties

An analysis of cloud radiative effect (CRE) for both SW (SWCRE) and LW (LWCRE), indicates a high global correlation between the mean CRE and climate sensitivity (Table 3). It is not obvious that this should be the case, and the spatial patterns between the SW and LW are different. The base-state CRE correlations with climate sensitivity (Figs. 6a,b) change sign between SW and LW (as for cloud feedback in Fig. 3). SWCRE is generally negative (Fig. 1a), and LWCRE is generally positive (Fig. 1b). This indicates that smaller-absolute-magnitude

TABLE 3. Table of correlations (corr) between γ_{eff} and listed state variables for CAM simulation pairs. Correlations that are statistically significant on the basis of a two-sided t test at the 95% level are marked with an asterisk. Also shown are the fraction of variance explained by the linear correlation (r^2 coefficient of determination) and the regression slope. Slope units in the first slope column are parameter units per kelvin, and they are percent per kelvin in the other columns. Values are shown for the mean parameter, the percent difference (% diff): $[(2 \times CO_2) - (1 \times CO_2)]/(1 \times CO_2)$, and the percent difference per degree kelvin of warming. Parameters are defined in the text.

Parameter	Units	Mean corr	r^2	Slope	% diff corr	r^2	Slope	% Diff K^{-1} corr	r^2	Slope
LWCRE	W m^{-2}	−0.82*	0.67	−2.8	−0.88*	0.79	−2.3	−0.86*	0.75	−0.54
SWCRE	W m^{-2}	0.64*	0.41	2.9	−0.96*	0.93	−3.1	−0.96*	0.92	−0.74
CLDLOW	Fraction	−0.07	0.01	−0.002	−0.70*	0.49	−3.1	−0.69*	0.48	−0.72
TWP	g m^{-2}	−0.82*	0.67	−25.0	−0.74*	0.55	−1.5	−0.75*	0.56	−0.87
LWP	g m^{-2}	−0.79*	0.62	−22.0	−0.65*	0.43	−3.4	−0.69*	0.47	−0.85
IWP	g m^{-2}	−0.39	0.15	−2.4	−0.65*	0.42	−2.1	−0.57*	0.33	−0.45
RH700	%	0.34	0.12	0.80	−0.69	0.47	−0.52	−0.66*	0.43	−0.11
LTS	K	−0.65*	0.43	−0.18	0.54*	0.29	0.39	0.44	0.19	0.08
ShCuMF	kg s^{-1}	0.43	0.19	0.001	−0.91*	0.82	−1.4	−0.81*	0.65	−0.30
DpCuMF	kg s^{-1}	0.40	0.16	0.002	−0.56*	0.31	−1.3	−0.55*	0.31	−0.30
REL860	μm	−0.71*	0.50	−0.63	0.88*	0.78	1.1	0.87*	0.70	0.23
NC860	m^{-3}	0.29	0.30	8.8×10^6	−0.75	0.54	−2.8	−0.74*	0.50	−0.48

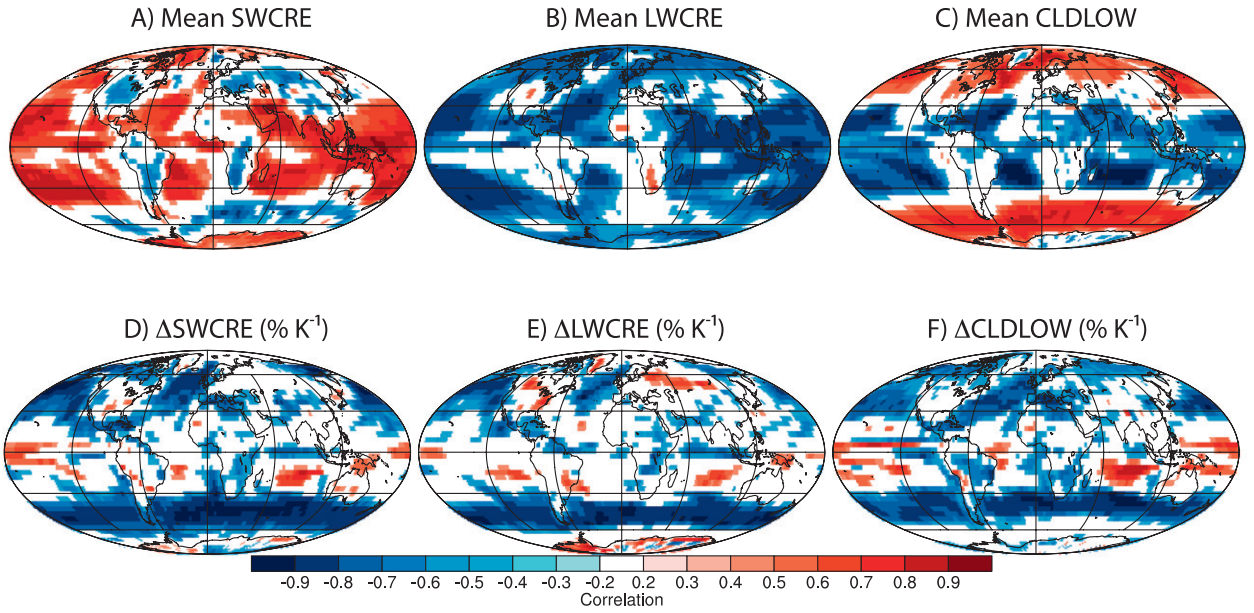

FIG. 6. Pattern correlations of γ_{eff} with (top) mean base ($1 \times CO_2$) state values and (bottom) percent differences (Δ%) per degree of local warming ΔT_s from 21 CAM experiments for (a),(d) SWCRE, (b),(e) LWCRE, and (c),(f) low cloud fraction.

SWCRE and LWCRE are correlated with higher climate sensitivity. Since the adjusted cloud feedback (Figs. 3a,b) and the CRE (Figs. 6d,e) correlations are similar, the correction for albedo effects (the difference between them) does not have a strong impact.

The pattern correlations of percent difference per degree of local warming (Figs. 6d,e) are very similar to the feedback patterns (Figs. 3a,b) but with a change in sign for the SW (because SWCRE is negative, the percent change is divided by a negative number). The pattern similarity indicates that the details of the regression method (including the regressor) do not strongly affect the identified regions. Although the feedback is ΔCRE/ΔT_s, here we examine ΔCRE/CRE/ΔT_s. The percent change in CRE per unit local warming is correlated with γ_{eff}, in the same regions where cloud feedbacks are correlated with γ_{eff}. An examination of correlation maps for the change in CRE calculated seasonally indicates that the correlations with sensitivity are slightly stronger in each hemisphere storm track in winter, similar to the zonal mean picture for feedbacks in Fig. 4. The pattern correspondence is a strong indication that the storm tracks are critical and that the radiative effects of clouds are important.

Changes in cloud frequency of occurrence are one component of cloud feedbacks (Zelinka et al. 2012b), and they have been used to assess feedbacks (e.g., Stephens 2005). Globally, percent-difference changes in low clouds (cloud-top $P > 700$ hPa; CLDLOW) are correlated with climate sensitivity while the mean state is not correlated (Table 3). The lack of global correlation results from opposite sign correlations between base ($1 \times CO_2$ state) CLDLOW and γ_{eff} with negative correlations over tropical oceans and positive correlations at middle and high latitudes (Fig. 6c). Higher γ_{eff} in the CESM experiments is associated with fewer base-state mean subtropical clouds and more high-latitude clouds.

The change in low cloud drives the overall change in total clouds and correlates strongly with sensitivity (Fig. 6f). Correlations for total cloudiness (not shown) are essentially the same. The local percent-difference pattern for low clouds (Fig. 6f), matches that for the response of SW CRE (Fig. 6d) and cloud feedbacks (Fig. 3c). The correspondence is consistent with the hypothesis that much of the signal in SWCRE contributing to cloud feedbacks is due to changes in areal extent at latitudes up to 60°N and 45°S. There is some signal in the subtropical stratocumulus transition regions in CLDLOW. However, changes at high Southern Hemisphere midlatitudes (45°–60°S in Fig. 6d) are not correlated with low cloud changes (Fig. 6f). Attribution of the cloud feedback to cloud-fraction changes in these regions is consistent with the interpretation of Zelinka et al. (2012b) from a suite of models from the CFMIP1 that cloud fraction changes are associated with the feedback changes at midlatitudes, but in some locations such as 45°–60°S other effects such as changes in cloud optical depth that are not related to fraction changes are important.

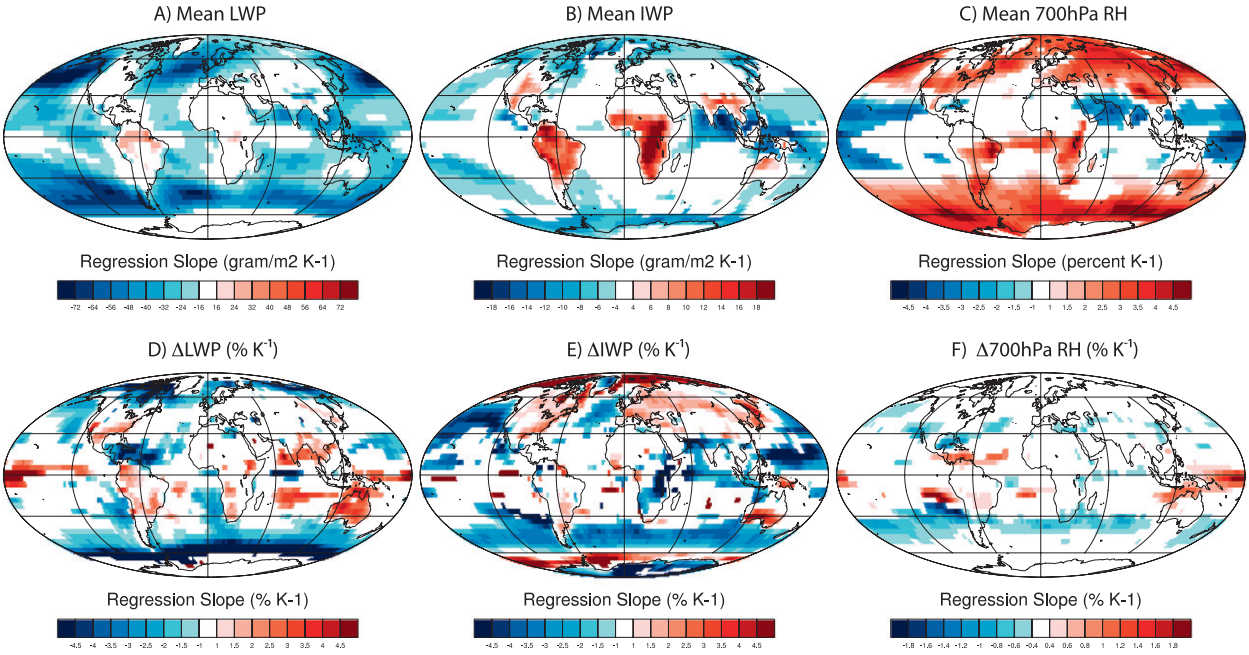

FIG. 7. Regression slope of γ_{eff} with (top) mean base ($1 \times CO_2$) state values and (bottom) percent differences ($\Delta\%$) per degree of local warming ΔT_s from 21 CAM experiments for (a),(d) LWP, (b),(e) IWP, and (c),(f) 700-hPa RH.

d. Moisture

Since water vapor is not correlated with sensitivity, and cloud radiative effect and cloud feedbacks are correlated, we next investigate condensed phase water. The condensed phase species in the atmosphere, diagnosed by the total condensed water path (TWP) and its components liquid water path (LWP) and ice water path (IWP), are strongly negatively correlated with climate sensitivity (Table 3) for both for the base state (except IWP) and the local percent perturbation. Water paths are gridbox averaged and represent the product of the in-cloud water path and total cloud fraction. Results for in-cloud TWP (and components) are similar. In general, TWP and LWP increase by 3%–6% in the $2 \times CO_2$ simulations while IWP decreases by 6%–10%, mostly in the storm tracks and at high latitudes.

The regression of LWP at each point against climate sensitivity is illustrated in Figs. 7a and 7d. Higher sensitivity occurs with a smaller mean LWP (Fig. 7a) in midlatitudes and a smaller percent increase in LWP in high latitudes of the Southern Hemisphere (Fig. 7d). Regressions over land are different because of different specification of deep convective ice and liquid water path over land and ocean in CESM. The base-state regression of LWP with γ_{eff} (Figs. 7a) reflects the cloud-feedback correlations (Fig. 3) and changes in CRE (Figs. 6d,e) and cloud fraction (Fig. 6f), suggesting that the change in CRE is associated with gridbox-averaged cloud-mass differences in the base state, particularly poleward of 40°N/S over oceans. An examination of individual seasons (Fig. 8a) indicates that correlations of base LWP and sensitivity are stronger in Northern Hemisphere summer whereas there is little difference in correlation by season in the Southern Hemisphere. The percent changes in LWP (Fig. 7d) have significant regression slope only in high latitudes, with some additional contribution from the stratocumulus transition regions of the subtropics. Smaller increases in LWP are correlated with increased sensitivity (less SW reflection and cooling by lower clouds).

For IWP (Figs. 7b,e), the regression of the base-state IWP with sensitivity is strongly positive over tropical land (because of the specification of convective IWP) and negative over tropical oceans as well as high latitudes. This implies thinner ice clouds over tropical oceans are associated with higher sensitivity. A similar pattern over ocean is seen in the percent changes of IWP (Fig. 7e) but with more prominence to the storm tracks, where larger decreases in IWP are associated with higher sensitivity, similar to feedback correlations (Fig. 3) and regressions (Fig. 5). The shifting balance between liquid and ice might be important, consistent with the effect suggested by Senior and Mitchell (1993) that melting ice to liquid (larger change in IWP) would mean enhanced sedimentation rates, less cloud, and larger negative cloud feedbacks (lower sensitivity). Shifts in ice-cloud regions were also noted by Tsushima et al.

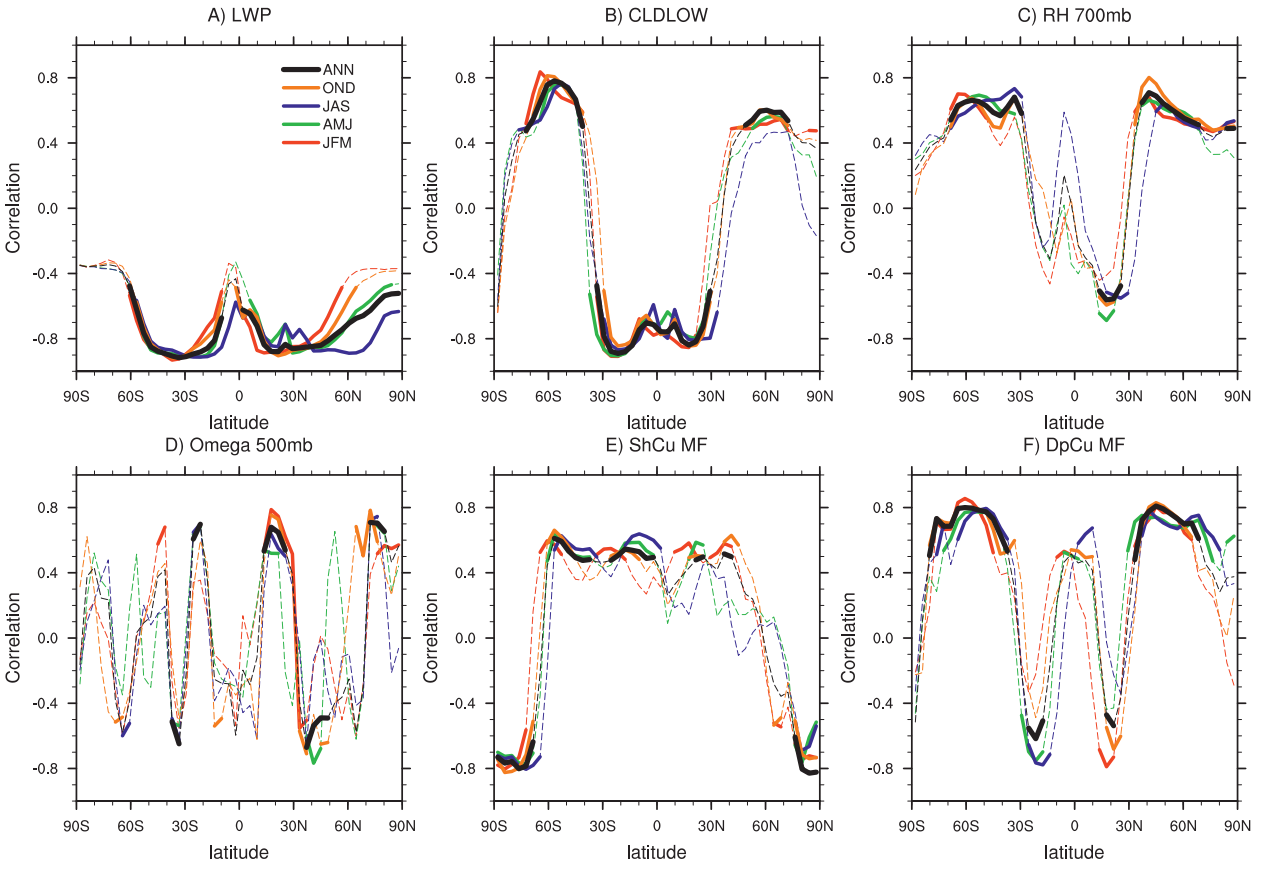

FIG. 8. Zonal mean seasonal correlations of γ_{eff} with cloud feedbacks at each point from 21 CAM experiments for (a) LWP, (b) CLDLOW, (c) RH700, (d) OMEGA500, (e) ShCuMF, and (f) DpCuMF. Thick lines are statistically significant. Annual means are shown in black.

(2006) and Ogura et al. (2008) as a contributor to differences in climate sensitivity.

There are also significant relationships between relative humidity (RH) and climate sensitivity, in both the base-state humidity (Fig. 7c) and the changes in RH (Fig. 7f). Here, 700-hPa conditions (RH700) are shown, but results are similar (although less significant), at lower pressures in the troposphere. Higher mean RH700 is associated with higher climate sensitivity, perhaps since higher RH, linked to cloud fraction through a parameterization (Slingo 1989), may make clouds more sensitive. Note that the mean RH is important at higher latitudes and near tropical convective regions. Changes in RH (Fig. 7f) have large slope only on the equatorward side of the storm tracks, indicating larger decreases in RH associated with higher sensitivity, consistent with regions of low cloud changes (Fig. 6f). No seasonality is seen in the mean correlations with RH700 (Fig. 8c). Tropical convective regions over ocean also are important for RH, reflecting changes to convective detrainment, which we examine in section 4e.

e. *Dynamics*

Of the feedbacks examined, cloud feedbacks have the highest correlations with climate sensitivity, and these correlations are consistent with changes to cloud radiative effect and changes in cloud fraction and liquid (and ice) water path. To better understand possible causes for the cloud changes, we next look at parameters describing atmospheric dynamics that are important for cloud processes. The following four metrics are explored: 1) lower-tropospheric stability [LTS, defined as the potential temperature θ difference between 700 hPa and the surface ($\theta_{700} - \theta_{\text{surface}}$)], 2) the midtropospheric (500 hPa) vertical velocity (OMEGA500), and the mass fluxes in the GCM convective parameterizations, divided into 3) deep (DpCuMF) and 4) shallow (ShCuMF) convective mass flux. The LTS and OMEGA500 metrics focus on the environmental dynamics that are important for low and stratus clouds, whereas the convective mass fluxes are diagnostics for changes in cumulus clouds. For ease of comparison, we use correlation maps (with the

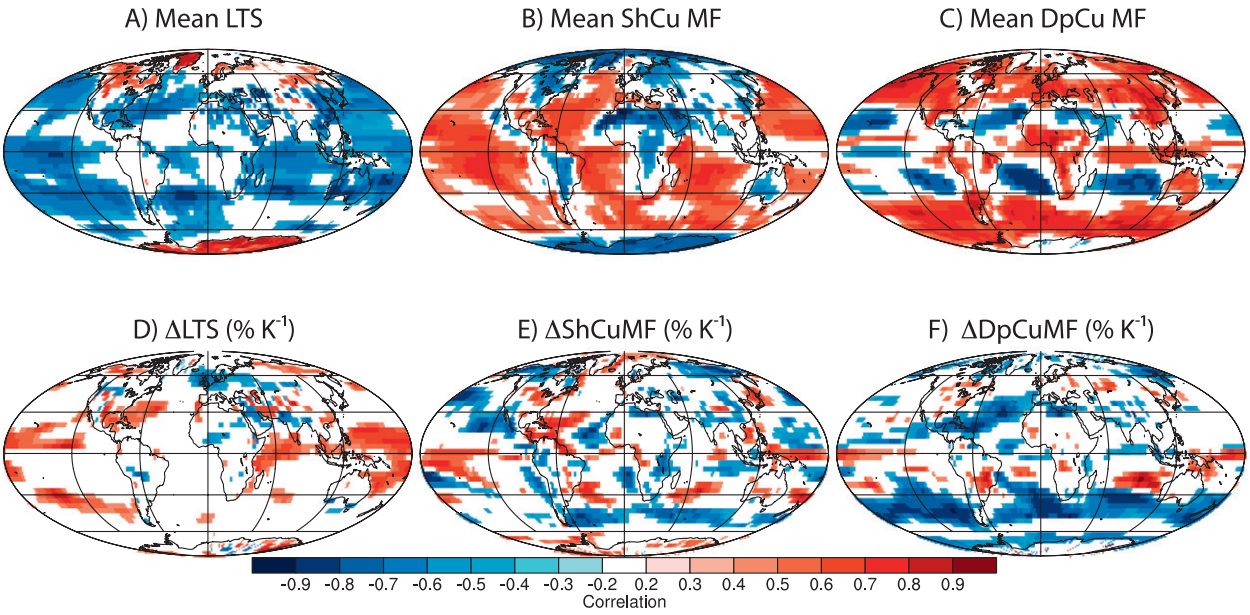

FIG. 9. Pattern correlations of γ_{eff} with (top) mean base ($1 \times CO_2$) state values and (bottom) (Δ%) per degree of local warming ΔT_s from 21 CAM experiments for (a),(d) LTS, (b),(e) ShCuMF, and (c),(f) DpCuMF.

same units), but the same information is provided by maps of regression slope.

The mean state of LTS is negatively correlated with climate sensitivity (Table 3 and Fig. 9a) mostly over ocean. Lower base-state stability is associated with higher climate sensitivity. The correlations peak on the equatorward part of the storm tracks, where base-state stability is low. The correlations with changes in LTS (Fig. 9d) are found only in limited regions of the subtropics, where larger percent increases in stability are associated with higher climate sensitivity on the flanks of deep convective regions. This may seem counterintuitive, but these dynamic changes may affect convection (see below) by altering the low-level instability that triggers parameterized convection.

The midtropospheric vertical velocity (OMEGA500) is regionally correlated with climate sensitivity (Fig. 8d). There are correlations of opposite sign over the tropical oceans with tropical upward motion (OMEGA500 < 0) associated with higher sensitivity. In the subtropics OMEGA500 > 0 is associated with higher sensitivity in regions that are similar to those associated with the LTS changes. This implies a relation between LTS and OMEGA500, but in the CESM simulations it does not translate into large changes in cloud feedbacks in the simulations as in other models (Soden and Vecchi 2011; Brient and Bony 2013), but rather it affects the equatorward edge of the storm tracks.

There are no significant global correlations between mean convective mass fluxes (DpCuMF and ShCuMF) and γ_{eff} (Table 3). This is because mean correlations with climate sensitivity show a regional dependence of different signs. Mean base-state ShCuMF over oceans (Fig. 9b) is positively correlated over oceans with climate sensitivity (larger mean flux correlated with higher sensitivity), with the opposite sign over land (also seen in the zonal mean in Fig. 8e). Part of the correlation arises from a fundamental change in CAM5 when a new shallow convective scheme was introduced. The introduction of this scheme significantly increased the climate sensitivity (Gettelman et al. 2012) while shallow convective mass flux increased globally. There are large percentage changes in ShCuMF that are correlated with sensitivity (Table 3), with decreases in ShCuMF associated with higher sensitivity. This is seen in the Southern Hemisphere storm track, but not as clearly, in Fig. 9e.

Base-state DpCuMF (Figs. 8f, 9c) is positively correlated with climate sensitivity over mid- and high latitudes but has negative correlations in the subtropics (where DpCuMF values are small). The subtropics have stronger regional correlations (Fig. 8f). Correlations of sensitivity with changes to convection are more coherent for deep convection than for shallow convection, particularly over the Southern Ocean (Fig. 9f), indicating smaller mass flux increases in this region in simulations with higher climate sensitivity (negative correlation). This is the same region where there are correlations between γ_{eff} and cloud feedbacks (Fig. 3), radiative effect (Figs. 6d,e), fraction (Fig. 6f), and water/ice path

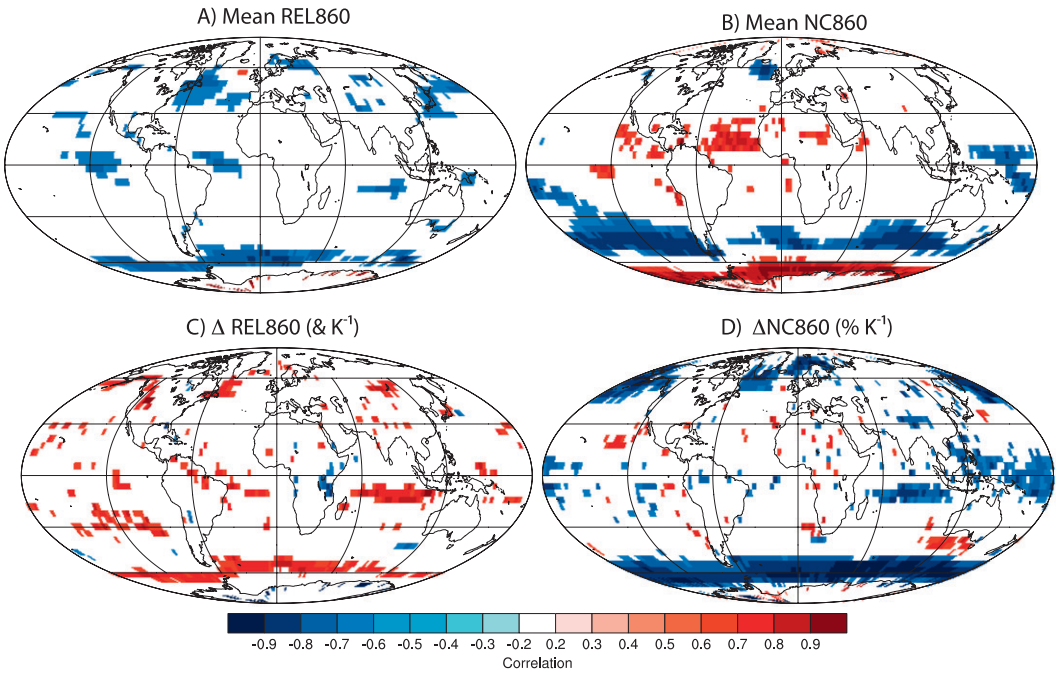

FIG. 10. Pattern correlations of γ_{eff} with (top) mean base ($1 \times CO_2$) state values and (bottom) (Δ%) per degree of local warming ΔT_s from 21 CAM experiments for (a),(c) REL860 and (b),(d) NC860.

(Figs. 7c,d). Mechanistically, deep and shallow convective clouds contain radiatively active water and detrain liquid and ice into stratiform clouds. More water in convective clouds in CAM means less available to stratiform clouds. Changes to convective fluxes will in turn affect cloud properties, radiative effects, and hence feedbacks. More deep and shallow convection (and larger change) results in reduced stratiform cloud mass and occurrence. This may also be combined with a poleward shift of these regions (and smaller areal extent). While mechanisms are hard to disentangle in CESM, it is clear that convective changes in the storm-track region that supply condensate to stratiform clouds are critical for the spread in climate sensitivity.

f. Microphysics

In addition to changes in cloud areal extent, changes to cloud radiative properties can be induced by changes to cloud microphysics. To diagnose these changes, we look at two related metrics for properties of low liquid clouds at 860 hPa near the top of the boundary layer: the 1) size (effective radius for liquid drops; REL860) and 2) number concentration of liquid drops (NC860). Radius and number are only available from 10 of 21 experiments with CAM5 microphysics. Therefore, here we are sampling variability only in part of the ensemble.

There is a significant negative global correlation between climate sensitivity and REL860 (Table 3). The slope ($-0.63\ \mu\text{m K}^{-1}$) is large given that the mean REL860 is about 10 μm. Correlations are concentrated in the storm-track regions (Figs. 10a,c), more poleward than the cloud fraction (Fig. 3f) correlations, but in a similar location to where the correlations of γ_{eff} with changes in liquid and ice water path are significant (Figs. 7c,d). The change may have to do with differences in partitioning between liquid and ice in a warmer world (more liquid in a warmer world), and the increases in droplet number concentrations occurring in polar regions as warming and poleward motion of the storm track occurs. These effects might simply be the microphysical result of other changes to the cloud environment. Consistent with this effect, Tsushima et al. (2006) found that changes in liquid–ice partitioning were important for changes in LWP leading to albedo and SW CRE changes related to climate sensitivity. Ogura et al. (2008) noted that the ice–liquid partitioning in the storm tracks was important for climate sensitivity in the Model for Interdisciplinary Research on Climate (MIROC) GCM.

The shift is illustrated in Fig. 10b, where larger γ_{eff} is associated with higher base-state NC860 at high southern latitudes and lower base-state NC860 at midsouthern latitudes. Thus, there is also no global correlation between base-state NC860 and climate sensitivity (Table 3) because of opposite regional signs. There are strong regional correlations of smaller increases in drop number

with increasing γ_{eff} in the simulations (Fig. 10d) at high latitudes, coincident with correlations and regression for smaller increases in liquid water path with increasing γ_{eff} (Fig. 7c). Thus, CESM simulations with high sensitivity tend to have lower mean LWP and smaller changes to LWP, along with smaller changes in NC860 and larger decreases in NC860 at high latitudes than simulations with low sensitivity. REL860 is not as coherent as cloud feedback or condensate correlations. The radiative effect of smaller changes in NC860 is to minimize any increase in SWCRE (reducing any cooling)—hence the contribution to increased sensitivity at these high latitudes poleward of the jet cores near 60°S/N. As noted however, correlation is not causation, and this might be a reaction to warmer temperatures (more melting, higher liquid fraction).

5. Discussion

Shortwave cloud feedback is known to be the largest source of intermodel spread in climate sensitivity (Bony et al. 2006; Soden and Vecchi 2011; Webb et al. 2012). In these CESM simulations, the strongest net cloud feedback correlations with climate sensitivity are found in the storm tracks of both hemispheres. These critical regions are different than in other recent work (Soden and Vecchi 2011) but are consistent with previous analyses of the predecessor model to CESM (Webb et al. 2012). Contributions from the subtropical stratocumulus transition regions are seen, but the net cloud feedback correlations in these regions are small. Using a larger ensemble than the differences between two models (CAM4 and CAM5) in Gettelman et al. (2012), the midlatitudes and subtropics are more prominent in determining the spread of climate sensitivity in CESM. To summarize, we discuss the result by regions and indicate possible mechanisms for these results in CESM.

The largest effects are seen in the storm tracks (30°–60°N/S). In the storm tracks, the spread of cloud feedbacks (Fig. 3) is related to climate sensitivity in the same regions as the changes to cloud radiative effect (Figs. 6d,e). Shortwave effects dominate (Figs. 3a, 6e), but the longwave effect plays an offsetting role (Fig. 3d). The biggest change in CESM occurs when a new shallow convective scheme is introduced (Gettelman et al. 2012, their Figs. 9 and 10). In the CESM simulations, the changes in cloud radiative effect (Fig. 6e) and changes in cloud fraction (Fig. 6f) are correlated with climate sensitivity on the equatorward side of the storm tracks. Thus, cloud-fraction changes (Fig. 6f) would seem to be the dominant effect, consistent with results by Zelinka et al. (2012b), and may be related to subtropical dry-zone expansion (Fasullo and Trenberth 2012). However, the meridional (poleward) motion of storm tracks seen with warming (Lu et al. 2009) is not correlated with sensitivity in the SOM experiments. CESM also has changes in deep convection on the equatorward flank of the storm tracks (Fig. 9f). Higher convective mass flux in higher-sensitivity experiments (Figs. 8d, 9c) lowers mean LWP and IWP by reducing condensate available to stratiform clouds (Fig. 7), tending to make cloud feedbacks more positive. Clouds may also be affected by and feed back on free tropospheric humidity in the region (Figs. 7f, 8c), and convection is tied to the strength of the tropical circulation (Fig. 8d), which is stronger (more gross upward and downward motion) in higher-sensitivity models. This illustrates the complex links between parameterizations and physical processes that affect feedbacks.

At high latitudes on the poleward flank of the jet (around 60°N/S) there are also relationships between cloud feedbacks and sensitivity (Fig. 3c). In these regions, smaller increases in low-cloud drop number (Fig. 10d) and LWP (Fig. 7b) are seen in higher-sensitivity CAM5 experiments. These changes may indicate that cloud properties (optical depth) and not cloud fraction may also affect feedbacks in these regions. The largest change in high-latitude feedbacks occurs when the new microphysics is introduced in CESM (Gettelman et al. 2012, their Figs. 9c and 10). The phase change between liquid and ice (Ogura et al. 2008) and the vertical motion (Fasullo and Trenberth 2012) in these regions may also be important. Note that cloud fraction in the region is already high. However, these areas are small. Adjusted cloud feedbacks in this region (Fig. 3c) may be sensitive to the surface albedo kernel around the sea ice edge. The uncertainty does not affect the changes in cloud parameters that are coherent with sensitivity in the high latitudes.

In the tropics and subtropics in CESM experiments, some evidence of relationships between global sensitivity and the cloud feedbacks in the stratocumulus and transition regions is seen (Figs. 3a, 5a). The changes to cloud microphysics also induce the largest change in cloud feedbacks in the tropics and subtropics (Gettelman et al. 2012, their Figs. 9c and 10). Regional analysis indicates that most of the spread in sensitivity in the CESM ensemble does not result from the tropics (within 30° of the equator). While deep convection is the same in all of these experiments, radiative (detrainment; ice cloud radiative properties) and dynamical (boundary layer structure) properties are very different in the tropics between CAM4 and CAM5, so it is not preordained that the tropical influence on the spread of feedbacks should be low. Cloud ice in the tropics does appear to be correlated with climate sensitivity (Figs. 7b,d), with less ice over ocean and more over land in the

base state associated with higher sensitivity. Larger decreases in ice in the subtropics are associated with higher sensitivity as well (Fig. 7d), but this does not seem to affect cloud feedback spread in the tropics. However, differences in base-state tropical and subtropical circulations (represented by OMEGA500 in Fig. 8e) indicate stronger tropical and subtropical overturning circulations in the base states associated with higher climate sensitivity, consistent with (Fasullo and Trenberth 2012). RH700 (Fig. 8c) is consistent with these changes, with lower RH in the subtropics and higher RH in midlatitudes correlated with higher sensitivity.

In CESM, the mean state appears to affect how clouds in the storm tracks change in response to CO_2-induced temperature changes. The changes appear to alter 1) the areal extent of shallow clouds and 2) the convective cloud mass flux on the equatorward branch of the storm tracks. Microphysics, by affecting cloud optical depth, plays a larger role on the poleward side of the storm track. The partitioning between the liquid and ice phases in this region may be important. The differences in climate sensitivity appear to be reflected in the mean state of cloud globally for condensed water mass and convective mass fluxes. Deep and shallow convective fluxes supply condensate to the stratiform clouds and so are also involved in altering cloud extent and condensate to impact cloud feedbacks. Higher mean convective fluxes occur when the new shallow convective scheme is introduced, and this is associated with reduced mean LWP by removing condensate. There are coherent correlations with tropical circulations and humidity associated with low clouds. In general, thinner clouds and stronger circulations are associated with higher sensitivity. This is expressed through changes in cloud fraction on the equatorward branch of the storm track and cloud condensate (and microphysics) within the storm track itself. Thinner clouds are more likely to experience large radiative changes and have larger feedbacks, even with the same CRE, for the reasons discussed below. The mechanism is similar to that seen in the MIROC GCM by Ogura et al. (2008), with larger changes in condensate in the storm tracks leading to larger cloud feedbacks and sensitivity, although the processes may be slightly different in CESM.

The relationship between LWP and cloud feedbacks illustrates the problem in using observations of cloud radiative effect to constrain models. All CESM simulations produce similar structures in CRE in present-day conditions (Fig. 1). CRE is a function of the cloud optical depth τ and cloud fraction a. The different model solutions have different a, and different Δa, but they also have different τ and $\Delta\tau$. Following Feingold and Siebert (2009), $\tau \propto N^{1/3} \times \mathrm{LWP}^{5/6}$ (where N is cloud drop number concentration). Thus, there can exist multiple combinations of N (or r_e, since $N \propto r_e^3$) and LWP to derive the same τ and CRE. Stated another way, CRE is a nonunique function of cloud cover a, the mass of condensate (LWP), and the particle size distribution (defined by number concentration N or effective radius r_e). Different base-state a, N, and LWP can yield the same base-state CRE, but the response of these properties to changes in surface temperature can be different. Thus, the perturbation to cloud radiative effect (and hence cloud feedbacks) is not well constrained by mean state CRE (e.g., Pincus et al. 2008), even though some relationships are seen in the global value in the CESM ensemble (Table 3). Furthermore, satellites have trouble distinguishing the N and LWP components of τ, resulting in large uncertainties in satellite-retrieved LWP (O'Dell et al. 2008; Seethala and Horváth 2010). With respect to the distribution of cloud τ in CESM, Kay et al. (2012a) illustrate that the mean state of clouds is closer to observations in CAM5 than in CAM4. The improvement results from the new two-moment microphysics and better consistency between cloud fraction and cloud water.

6. Conclusions

CESM experiments analyzed here confirm that SW cloud feedbacks are critical for understanding climate sensitivity. The different factors that go into the spread of cloud feedbacks have been examined by location and related to parameters describing the properties of clouds. The key feedback regions correlated with climate sensitivity in CESM are the midlatitude storm tracks extending into the subtropics. In these regions, CRE also is correlated with climate sensitivity. On the equatorward branch of the storm tracks, the correlation is coherent with mean base-state water content. Decreases in mean water content are collocated with increases to the mean convective supply of moisture in these regions that occurs when a new shallow convective scheme is introduced. At high latitudes, there appears to be evidence of differences in cloud properties (number concentration) and LWP that are correlated with the spread in sensitivity or perhaps a result of changes in liquid and ice partitioning.

Finding the ultimate ''cause'' of the difference in climate sensitivity among these simulations is elusive. Regression analysis does not provide causation, only correlation. We have sketched a coherent picture from the CESM ensemble that indicates cloud feedbacks in specific regions (subtropics and midlatitudes) are critical. The sensitivity and the feedbacks are a result of specific processes that seem linked to changes in cloud

frequency of occurrence and the supply of moisture through the general circulation (vertical velocity) and convective mass fluxes and are related to the environmental humidity. At higher latitudes, mean condensate and changes to number concentrations are important. This may be a result of shifts in the liquid and ice balance.

The results above have been derived by use of two different parameterization suites in a GCM (CAM4 and CAM5) within the same coupled model framework (CESM). The results are not strongly sensitive to how the simulations are analyzed. The cloud response appears to be identical in a fixed-SST-only experiment (no CO_2 changes), indicating that the response is a slow feedback response. The critical regions (the midlatitude storm tracks) are very different than regions where spread is seen in other model frameworks (e.g., Soden and Vecchi 2011; Webb et al. 2012), where they have been related to boundary layer changes (Brient and Bony 2013). However, the strong spread of sensitivity in the storm tracks is consistent with strong cloud feedbacks in these regions (Zelinka et al. 2012b). These changes are also consistent with the decomposition of cloud feedback by cloud fraction and cloud properties by Zelinka et al. (2012b). The results here are also consistent with CCSM3 results by Webb et al. (2012), the importance of the storm tracks in MIROC seen by Ogura et al. (2008), and correlations between climate sensitivity and absorbed solar radiation in the Southern Ocean reported by Trenberth and Fasullo (2010). Ultimately the focus in CESM appears to be low clouds in the equatorward part of the storm tracks, but these seem strongly affected by changes in the shallow convection scheme, which significantly alters the mean state of clouds and condensate, but with the same base CRE. Other studies have also noted the importance of the convection scheme for climate feedbacks (Taylor et al. 2011a).

The CESM relationship in midlatitudes has a strong physical basis in the nonunique relationship between cloud optical depth and cloud radiative effect that may confound our ability to constrain the microphysical components (N; LWP) of cloud optical depth that defines CRE. It is thus not surprising that similar CRE can respond to changes in surface temperature differently, yielding different cloud feedbacks and climate sensitivity.

Further work will extend this analysis to other model systems. The difference between CESM results and those of other single-model or multimodel analyses, particularly those using similar methods (e.g., Soden and Vecchi 2011) provides a very interesting avenue to explore why cloud feedbacks are different. However, Klocke et al. (2011) highlight that statistical relationships to present-day states in a single-model ensemble do not seem to translate to a multiple-model ensemble. The focus has been on radiative properties of the system (CRE) that are nonunique functions of physical properties (LWP and IWP). Thus, care must be taken to link relationships to physical properties of the system that are well constrained beyond just regression analysis. CRE is well observed but not well constrained. Comparisons with observations, for example, through the use of satellite simulators (Bodas-Salcedo et al. 2011), are helping to constrain the properties of present-day clouds better (Kay et al. 2012a) and may yield additional constraints on climate feedbacks and climate sensitivity.

Acknowledgments. Computing resources were provided by the Climate Simulation Laboratory at the NCAR Computational and Information Systems Laboratory. NCAR is sponsored by the U.S. National Science Foundation. Doctor Fasullo's research was sponsored by NASA Awards NNX09AH89G-S01 and NNG06GB91G. Thanks are given to K. M. Shell, J. T. Kiehl, G. A. Meehl, B. P. Medeiros, and B. N. Sanderson for comments.

APPENDIX

CAM Experiment Details

CAM experiments contain a total of 8 SOM experiments and 13 standalone experiments, listed in Table 1. Each experiment is two simulations, with different values of CO_2. SOM configurations follow Bitz et al. (2012), with specified deep ocean heat fluxes, and are run for 60 yr, with the last 20 yr analyzed. Atmosphere-only model experiments have a perturbed SST for the $2 \times CO_2$ case specified in addition to the change in CO_2 concentration. These ''modified Cess'' experiments are described by Gettelman et al. (2012) and are similar to $\pm$2-K perturbation experiments originally described by Cess et al. (1989). Modified Cess experiments have a patterned SST perturbation and are run for 5 or 10 yr. Feedbacks averaged over 5 or 10 yr are the same, and therefore the results are not sensitive to experiment length. SOM (Knutti et al. 2006) and SST perturbation experiments (Gettelman et al. 2012) can reproduce climate feedbacks and climate sensitivity in coupled atmosphere–ocean simulations.

Experiment pairs are performed with CAM4 physics (Neale et al. 2008) or CAM5 physics (Gettelman et al. 2010; Neale et al. 2010). There is one SOM run for each model (CAM4-SOM; CAM5-SOM) at $0.9° \times 1.25°$ horizontal resolution and one at $1.9° \times 2.5°$ (-SOM2). Results are not sensitive to these different resolutions (Gettelman et al. 2012). There are three different parameter adjustment experiments of CAM5-SOM2 with interim versions of the model, but with a host of

different changes to the physics suite, labeled $\alpha 1$–$\alpha 3$. These represent different experiments altering ice nucleation, ice autoconversion, and convective cloud water partitioning along with adjustment of the energy balance with changes to the relative humidity threshold for stratiform cloud formation (see below). These experiments have a wide range of sensitivity in Table 1. There is one run of the CAM5 physics with year-1850 aerosols (CAM5-SOMa) designed to see if the aerosols affect sensitivity. All other SOM runs use year-2000 aerosols. In addition, there is a suite of $1.9° \times 2.5°$ modified Cess (fixed SST perturbation) experiments that describe the changes in parameterizations between CAM4 (CAM4-Cess) and CAM5 (CAM5-Cess). These are listed sequentially in Table 1. Two of these experiments (+micro2, +PBL2) have modified parameters for cloud formation thresholds (RH_c), designed to better close the planetary energy balance that allows testing of the impact of this tuning on sensitivity. Another experiment (Conv) has perturbed the partitioning of LWP in convection over land. These were designed to see whether single parameter adjustments affected sensitivity (they do not). Last, there are modified Cess experiments with fixed aerosol mass (Aero) and an SST perturbation from a CAM4-SOM Run (ΔSST4); other runs use ΔSST from CAM5-SOM. This experiment explores whether the simulation setup alters sensitivity (not strongly).

REFERENCES

Bitz, C., K. M. Shell, P. R. Gent, D. Bailey, G. Danabasoglu, K. C. Armour, M. M. Holland, and J. T. Kiehl, 2012: Climate sensitivity of the Community Climate System Model, version 4. *J. Climate,* **25,** 3053–3070.

Bodas-Salcedo, A., and Coauthors, 2011: COSP: Satellite simulation software for model assessment. *Bull. Amer. Meteor. Soc.,* **92,** 1023–1043.

Bony, S., and Coauthors, 2006: How well do we understand and evaluate climate change feedback processes? *J. Climate,* **19,** 3445–3482.

Brient, F., and S. Bony, 2013: Interpretation of the positive low-cloud feedback predicted by a climate model under global warming. *Climate Dyn.,* **40,** 2415–2431, doi:10.1007/s00382-011-1279-7.

Cess, R. D., and Coauthors, 1989: Interpretation of cloud-climate feedback as produced by 14 atmospheric general circulation models. *Science,* **245,** 513–516.

Charney, J. G., 1979: Carbon dioxide and climate: A scientific assessment. National Academy of Science Tech. Rep., 22 pp. [Available online at http://www.nap.edu/catalog.php?record_id=12181.]

Collins, W. D., and Coauthors, 2004: Description of the NCAR Community Atmosphere Model (CAM3.0). NCAR Tech. Note NCAR/TN-464+STR, 214 pp. [Available online at http://www.cesm.ucar.edu/models/atm-cam/docs/description/description.pdf.]

——, and Coauthors, 2006: The formulation and atmospheric simulation of the Community Atmosphere Model: CAM3. *J. Climate,* **19,** 2122–2161.

Colman, R., 2002: Geographical contributions to global climate sensitivity in a general circulation model. *Global Planet. Change,* **32,** 211–243.

——, 2003: A comparison of climate feedbacks in general circulation models. *Climate Dyn.,* **20,** 865–873.

Dessler, A. E., 2010: A determination of the cloud feedback from climate variations over the past decade. *Science,* **330,** 1523–1527.

Dufresne, J.-L., and S. Bony, 2008: An assessment of the primary sources of spread of global warming estimates from coupled atmosphere–ocean models. *J. Climate,* **21,** 5135–5144.

Fasullo, J. T., and K. E. Trenberth, 2012: A less cloudy future: The role of subtropical subsidence in climate sensitivity. *Science,* **338,** 792–794.

Feingold, G., and H. Siebert, 2009: Cloud–aerosol interactions from the micro to the cloud scale. *Clouds in the Perturbed Climate System,* J. Heintzenberg and R. J. Charlson, Eds., MIT Press, 319–338.

Flanner, M. G., K. M. Shell, M. Barlage, D. K. Perovich, and M. A. Tschudi, 2011: Radiative forcing and albedo feedback from the Northern Hemisphere cryosphere between 1979 and 2008. *Nat. Geosci.,* **4,** 151–155.

Gettelman, A., and Q. Fu, 2008: Observed and simulated upper-tropospheric water vapor feedbacks. *J. Climate,* **21,** 3282–3289.

——, and Coauthors, 2010: Global simulations of ice nucleation and ice supersaturation with an improved cloud scheme in the Community Atmosphere Model. *J. Geophys. Res.,* **115,** D18216, doi:10.1029/2009JD013797.

——, J. E. Kay, and K. M. Shell, 2012: The evolution of climate feedbacks in the Community Atmosphere Model. *J. Climate,* **25,** 1453–1469.

Gregory, J., and M. Webb, 2008: Tropospheric adjustment induces a cloud component in CO_2 forcing. *J. Climate,* **21,** 58–71.

Hansen, J., and Coauthors, 2002: Climate forcings in Goddard Institute for Space Studies SI2000 simulations. *J. Geophys. Res.,* **107,** 4347, doi:10.1029/2001JD001143.

Huber, M., I. Mahlstein, M. Wild, J. Fasullo, and R. Knutti, 2011: Constraints on climate sensitivity from radiation patterns in climate models. *J. Climate,* **24,** 1034–1052.

Kay, J. E., and Coauthors, 2012a: Exposing global cloud biases in the Community Atmosphere Model (CAM) using satellite observations and their corresponding instrument simulators. *J. Climate,* **25,** 5190–5207.

——, M. M. Holland, H. C. Bitz, A. Gettelman, E. Blanchard-Wrigglesworth, A. Conley, and D. Bailey, 2012b: The influence of local feedbacks and northward heat transport on the equilibrium Arctic climate response to increased greenhouse gas forcing. *J. Climate,* **25,** 5433–5450.

Klocke, D., R. Pincus, and J. Quaas, 2011: On constraining estimates of climate sensitivity with present-day observations through model weighting. *J. Climate,* **24,** 6092–6099.

Knutti, R., G. A. Meehl, M. R. Allen, and D. A. Stainforth, 2006: Constraining climate sensitivity from the seasonal cycle in surface temperature. *J. Climate,* **19,** 4224–4233.

Loeb, N. G., B. A. Wielicki, D. R. Doelling, G. L. Smith, D. F. Keyes, S. Kato, N. M. Smith, and T. Wong, 2009: Towards optimal closure of the earth's top-of-atmosphere radiation budget. *J. Climate,* **22,** 748–766.

Lu, J., C. Deser, and T. Reichler, 2009: Cause of the widening of the tropical belt since 1958. *Geophys. Res. Lett.,* **36,** L03803, doi:10.1029/2008GL036076.

Meehl, G. A., C. Covey, K. E. Taylor, T. Delworth, R. J. Stouffer, M. Latif, B. McAvaney, and J. F. B. Mitchell, 2007a: The

WCRP CMIP3 multimodel dataset: A new era in climate change research. *Bull. Amer. Meteor. Soc.,* **88,** 1383–1394.

——, and Coauthors, 2007b: Global climate projections. *Climate Change 2007: The Physical Science Basis,* S. Solomon et al., Eds., Cambridge University Press, 747–845.

Neale, R. B., J. H. Richter, and M. Jochum, 2008: The impact of convection on ENSO: From a delayed oscillator to a series of events. *J. Climate,* **21,** 5904–5924.

——, and Coauthors, 2010: Description of the NCAR Community Atmosphere Model (CAM5.0). NCAR Tech. Note NCAR/TN-486+STR, 268 pp. [Available online at http://www.cesm.ucar.edu/models/cesm1.1/cam/docs/description/cam5_desc.pdf.]

O'Dell, C. W., F. J. Wentz, and R. Bennartz, 2008: Cloud liquid water path from satellite-based passive microwave observations: A new climatology over the global oceans. *J. Climate,* **21,** 1721–1739.

Ogura, T., S. Emori, M. J. Webb, Y. Tsushima, T. Yokohata, A. Abe-Ouchi, and M. Kimoto, 2008: Towards understanding cloud response in atmospheric GCMs: The use of tendency diagnostics. *J. Meteor. Soc. Japan,* **86,** 69–79.

Piani, C., D. J. Fraame, D. A. Stainforth, and M. R. Allen, 2005: Constraints on climate change from a multi-thousand member ensemble of simulations. *Geophys. Res. Lett.,* **32,** L23825, doi:10.1029/2005GL024452.

Pincus, R., C. P. Batstone, R. J. P. Hoffman, K. E. Taylor, and P. J. Glecker, 2008: Evaluating the present-day simulation of clouds, precipitation and radiation in climate models. *J. Geophys. Res.,* **113,** D14209, doi:10.1029/2007JD009334.

Rougier, J., D. M. H. Sexton, J. M. Murphy, and D. Stainforth, 2009: Analyzing the climate sensitivity of the HadSM3 climate model using ensembles from different but related experiments. *J. Climate,* **22,** 3540–3557.

Sanderson, B. M., and K. M. Shell, 2012: Model-specific radiative kernels for calculating cloud and non-cloud climate feedbacks. *J. Climate,* **25,** 7607–7624.

——, C. Piani, W. J. Ingram, D. A. Stone, and M. R. Allen, 2008: Towards constraining climate sensitivity by linear analysis of feedback patterns in thousands of perturbed-physics GCM simulations. *Climate Dyn.,* **30,** 175–190.

——, K. M. Shell, and W. Ingram, 2010: Climate feedbacks determined using radiative kernels in a multi-thousand member ensemble of AOGCMs. *Climate Dyn.,* **35,** 1219–1236.

Seethala, C., and A. Horváth, 2010: Global assessment of AMSR-E and MODIS cloud liquid water path retrievals in warm oceanic clouds. *J. Geophys. Res.,* **115,** D13202, doi:10.1029/2009JD012662.

Senior, C. A., and J. F. B. Mitchell, 1993: Carbon dioxide and climate: The impact of cloud parameterization. *J. Climate,* **6,** 393–418.

Shell, K. M., J. T. Kiehl, and C. A. Shields, 2008: Using the radiative kernel technique to calculate climate feedbacks in NCAR's Community Atmosphere Model. *J. Climate,* **21,** 2269–2282.

Slingo, A. A., 1989: A GCM parameterization for the shortwave radiative properties of clouds. *J. Atmos. Sci.,* **46,** 1419–1427.

Soden, B. J., and I. M. Held, 2006: An assessment of climate feedbacks in coupled ocean–atmosphere models. *J. Climate,* **19,** 3354–3360.

——, and G. A. Vecchi, 2011: The vertical distribution of cloud feedback in coupled ocean–atmosphere models. *Geophys. Res. Lett.,* **38,** L12704, doi:10.1029/2011GL047632.

——, R. T. Wetherald, G. L. Stenchikov, and A. Robock, 2002: Global cooling after the eruption of Mount Pinatubo: A test of climate feedback by water vapor. *Science,* **296,** 727–730.

——, I. M. Held, R. Colman, K. M. Shell, J. T. Kiehl, and C. A. Shields, 2008: Quantifying climate feedbacks using radiative kernels. *J. Climate,* **21,** 3504–3520.

Solomon, S., D. Qin, M. Manning, Z. Chen, M. Marquis, K. Averyt, M. Tignor, and H. L. Miller Jr., Eds., 2007: *Climate Change 2007: The Physical Science Basis.* Cambridge University Press, 996 pp.

Stephens, G. L., 2005: Cloud feedbacks in the climate system: A critical review. *J. Climate,* **18,** 237–273.

Taylor, P. C., R. G. Ellingson, and M. Cai, 2011a: Geographical distribution of climate feedbacks in the NCAR CCSM3.0. *J. Climate,* **24,** 2737–2753.

——, ——, and ——, 2011b: Seasonal variation of climate feedbacks in the NCAR CCSM3.0. *J. Climate,* **24,** 3433–3444.

Trenberth, K. E., and J. T. Fasullo, 2010: Simulation of present-day and twenty-first-century energy budgets of the southern oceans. *J. Climate,* **23,** 440–454

Tsushima, Y., and Coauthors, 2006: Importance of the mixed-phase cloud distribution in the control climate for assessing the response of clouds to carbon dioxide increase: A multi-model study. *Climate Dyn.,* **27,** 113–126.

Watanabe, M., and Coauthors, 2012: Using a multiphysics ensemble for exploring diversity in cloud shortwave feedback in GCMs. *J. Climate,* **25,** 5416–5431.

Webb, M. J., and Coauthors, 2006: On the contribution of local feedback mechanism to the range of climate sensitivity in two GCM ensembles. *Climate Dyn.,* **27,** 17–38.

——, F. H. Lambert, and J. M. Gregory, 2012: Origins of differences in climate sensitivity, forcing and feedback in climate models. *Climate Dyn.,* **38,** 677–707, doi:10.1007/s00382-012-1336-x.

Williams, K. D., and M. J. Webb, 2009: A quantitative performance assessment of cloud regimes in climate models. *Climate Dyn.,* **33,** 141–157.

Yoshimori, M., J. C. Hargreaves, J. D. Annan, T. Yokohata, and A. A. Ouchi, 2011: Dependency of feedbacks on forcing and climate state in physics parameter ensembles. *J. Climate,* **24,** 6440–6455.

Zelinka, M. D., and D. L. Hartmann, 2010: Why is longwave cloud feedback positive? *J. Geophys. Res.,* **115,** D16117, doi:10.1029/2010JD013817.

——, S. A. Klein, and D. L. Hartmann, 2012a: Computing and partitioning cloud feedbacks using cloud property histograms. Part I: Cloud radiative kernels. *J. Climate,* **25,** 608–624.

——, ——, and ——, 2012b: Computing and partitioning cloud feedbacks using cloud property histograms. Part II: Attribution to changes in cloud amount, altitude, and optical depth. *J. Climate,* **25,** 3736–3754.